The Astrophysical Journal, 893:71 (8pp), 2020 April 10 https://doi.org/10.3847/1538-4357/ab7e2b
© 2020. The American Astronomical Society. All rights reserved.

Proton Perpendicular Heating in Turbulence Simulations: Determination of the Velocity Diffusion Coefficient

Bernard J. Vasquez, Philip A. Isenberg, and Sergei A. Markovskii
Space Science Center, University of New Hampshire, Durham, NH 03824, USA; bernie.vasquez@unh.edu, phil.isenberg@unh.edu, sergei.markovskii@unh.edu
Received 2020 February 7; revised 2020 March 6; accepted 2020 March 8; published 2020 April 16

Abstract

Numerical methods are presented that can determine the perpendicular velocity space diffusion coefficient from kinetic simulation results. The methods are applied to hybrid simulation results using particle protons and a massless, quasi-neutralizing electron fluid for a case of quasi-perpendicular turbulence. During the quasi-steady phase of the turbulence, the evolution of the grid-averaged, gyrotropic, and peculiar velocity distribution of protons with velocity components perpendicular to the background magnetic field is found to be adequately described by diffusion. The estimated diffusion coefficient varies with perpendicular proton speed. A relative maximum occurs at a speed of zero. About the thermal speed, the coefficient decreases with increasing speed consistent with a power law with index −3. A relative minimum occurs at larger speeds, and the diffusion coefficient rises among the fastest protons contained in the simulation. The functional form of the diffusion coefficient appears to be the result of two sources. At speeds less than the relative minimum, the diffusion is dominated by turbulence generated fluctuations, while at greater speeds the diffusion arises from the large-scale fluctuations that initiated the turbulent energy cascade. Results are compared with theoretical predictions for the diffusion coefficient and with results presented from a previous simulation. Implications for generating suprathermal protons from quasi-perpendicular turbulence are also discussed.

Unified Astronomy Thesaurus concepts: Solar wind (1534); Interplanetary turbulence (830); Space plasmas (1544)

1. Introduction

Interplanetary turbulence largely heats the solar wind protons near 1 au (e.g., Verma et al. 1995; Vasquez et al. 2007; Stawarz et al. 2009; Coburn et al. 2012; Hellinger et al. 2013; Lamarche et al. 2014). Near the Sun, the turbulent energy cascade could also be an important factor in forming the solar wind, contributing both thermal energy and bulk acceleration (e.g., Hollweg 1986; Hollweg & Johnson 1988; Dmitruk et al. 2003; Cranmer & van Ballegooijen 2005). Kinetic processes must be involved in the heating since a turbulence dissipation range forms at proton kinetic scales and nonthermal ion distributions are observed (e.g., Marsch et al. 1982; Kohl et al. 1998; Leamon et al. 1998; Hamilton et al. 2008; Smith et al. 2012; Hellinger et al. 2013). Proton heating in the solar wind is mostly perpendicular to the background magnetic field and opposes the adiabatic cooling with increasing heliocentric distance in a spherically expanding wind (Marsch et al. 1983; Hellinger et al. 2013).

In order for simulations to examine the processes of dissipating the energy cascade and heating the solar wind, the proton kinetic scales must be resolved. This required resolution does not allow the inclusion of the spatial dependency of the heating and acceleration of the solar wind that arises for much larger scales. Calculations that treat the larger scales of the wind can be made with a less complete description of the kinetic physics. One such approach uses a guiding center treatment of the ions and includes the kinetic effects through diffusion coefficients based on fluctuation–ion interactions (e.g., Isenberg & Vasquez 2009, 2011, 2015).

Alfvénic turbulence in the interplanetary medium is known to energize primarily fluctuations with wavevectors that are mostly perpendicular to the background magnetic field (e.g., Shebalin et al. 1983; Oughton et al. 1994; Matthaeus et al. 1998; Cho & Vishniac 2000; Vasquez et al. 2014). In accord with solar wind observations, kinetic simulations have shown that protons are heated perpendicularly in association with these cascades although the mechanism for this heating is not definitively known (e.g., Parashar et al. 2009; Vasquez & Markovskii 2012; Vasquez 2015; Yang et al. 2017). Two processes have been considered that model this heating as a perpendicular diffusion. One is stochastic heating, which is also referred to as magnetic moment breaking, wherein electric field variations from fluctuations about the gyroscale of the ions, scatter the ions and lead to a net gain of energy at the expense of the fluctuations (e.g., Chandran et al. 2010; Klein & Chandran 2016; Isenberg et al. 2019). The second mechanism involves kinetic Alfvén wave cyclotron resonant damping on ions (Isenberg & Vasquez 2019). In this view the energy cascade produces fluctuations that, at least in part, mimic these waves for a short duration, but long enough that a quasilinear diffusion coefficient (e.g., Kennel & Engelmann 1966) for the resonant waves can be applied.

By averaging over the gyration spatial scales, an estimate of the diffusion coefficient from kinetic simulation results can be made. The coefficient can be compared with existing predictions and be incorporated into calculations of solar wind heating and acceleration. Arzamasskiy et al. (2019) conducted hybrid simulations with particle protons and fluid electrons for quasi-perpendicular turbulence and presented proton energy diffusion coefficients derived from these simulations. However, their analysis neglected a significant term and did not consider the sign of the remaining term. We will discuss these results in Section 4.

In the present analysis, the numerical methodology to obtain a velocity or energy diffusion coefficient from kinetic simulations is outlined that neglects neither sign nor terms. The results are applied to a well studied case in Vasquez (2015) of quasi-perpendicular turbulence using hybrid numerical

simulations. The velocity diffusion coefficient maximizes at zero speed and then declines sharply above the thermal speed. A subsequent increase in the diffusion coefficient at the largest proton speeds is likely due to interactions with the large-scale fluctuations that include the initial seed spectrum of the turbulence.

The outline of this paper is as follows: Section 2 briefly describes the particular simulation run to be examined. The numerical methods and simulation results for the diffusion coefficient are given in Section 3. The method used in Arzamasskiy et al. (2019) is discussed in Section 4, and Section 5 addresses the production of suprathermal protons. Section 6 summarizes the methods and findings.

2. Simulation Parameters

Three-dimensional hybrid numerical simulations have been carried out with particle protons and a quasi-neutralizing, massless electron fluid to investigate the development of quasi-perpendicular turbulence. This paper considers run IVb in Vasquez (2015) as a representative example. In this run, the grid has 256^3 cells. Along the x direction is a constant background magnetic field $\boldsymbol{B}_0$, and here the grid length $L_\parallel$, normalized by proton inertial lengths $c/\omega_{\rm pp}$, is 142.16, where c is the speed of light and $\omega_{\rm pp}$ is the proton plasma frequency. Along the perpendicular directions y and z, the grid length $L_\perp$ is 25.13 so that the aspect ratio of the grid $L_\parallel/L_\perp$ is 5.66. Triply periodic boundary conditions are used.

The initial proton plasma has a uniform density with 200 particles per cell. The ratio of proton to magnetic pressure $\beta_{\rm p}$ is set to 0.1. The electron pressure is neglected to emphasize ion kinetic effects.

The initial fluctuations are energized at the lowest modes and have fluctuating bulk velocities and magnetic fields in accord with Alfvén waves. The initial proton distribution is a Maxwellian about the spatially varying bulk velocity. The initial rms of the combined average of the velocity fluctuations and magnetic field fluctuations in Alfvén units is 0.17 $V_{\rm A}^2$, where $V_{\rm A}$ is the background Alfvén speed. The developed turbulence is freely decaying.

3. Results for the Diffusion Coefficient

Figure 1 shows the change with time in the parallel $\Delta W_{\rm ther,\parallel}$ and perpendicular $\Delta W_{\rm ther,\perp}$ thermal energy density averaged over the entire grid. The thermal energy densities are normalized by $n_0 m_p V_{\rm A}^2$ where n_0 is the background proton number density and $m_{\rm p}$ is the proton mass. The parallel and perpendicular directions are with respect to $\boldsymbol{B}_0$. The proton thermal energy or temperature is assessed from the peculiar distribution function where the bulk velocity at each particle position has been removed from its total velocity. The quasi-steady turbulent phase begins after 80 $\Omega_{\rm p}^{-1}$ where $\Omega_{\rm p}$ is the angular proton cyclotron frequency. Most of the heating occurs perpendicular to $\boldsymbol{B}_0$. The heating slows after 300 $\Omega_{\rm p}^{-1}$ because the turbulent fluctuations decay.

Near and below $c/\omega_{\rm pp}$, electric field gradient effects produce nongyrotropic peculiar distribution functions about the local magnetic field that vary with position. When the peculiar velocity distribution is computed for the entire grid, whose lengths well exceed $c/\omega_{\rm pp}$, the cancellation will average away the local variations of nongyrotropy about $\boldsymbol{B}_0$. Comparison of the bin velocity distribution in v_y and v_z, integrated over the grid, confirms this result. There do remain bin-scale fluctuations in the calculated distributions due to finite particle numbers. Numerically, the optimal estimate of the gyrotropically averaged distribution can be gained first by finding the distribution based on combined y and z components of speed and then calculating from that an average gyrotropic distribution.

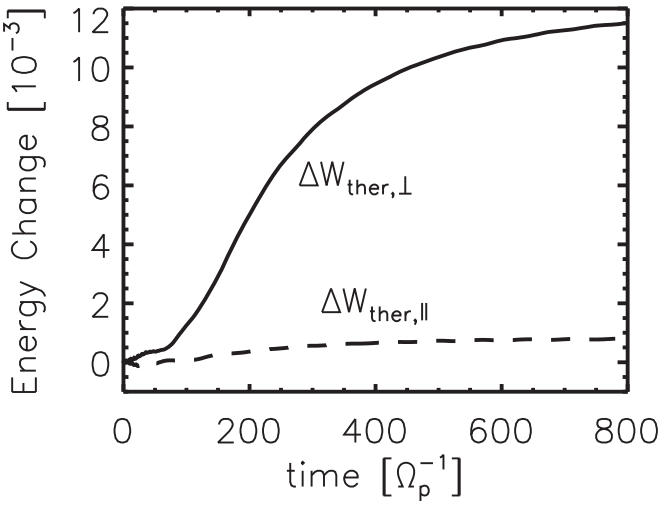

Figure 1. Change from the initial time in the space averaged proton thermal energy density as a function of time. Parallel thermal energy is plotted with a dashed line and perpendicular with a solid line. The initial total thermal energy density is $0.075 n_0 m_p V_{\rm A}^2$, and the value of $\beta_{\rm p}$ is 0.1. The sum of fluctuating magnetic energy and total proton energy is conserved to better than 0.06%.

Proton particle speeds v_r perpendicular to $\boldsymbol{B}_0$ are determined by $v_r = (v_y^2 + v_z^2)^{1/2}$. Hereinafter, all speeds are normalized by $V_{\rm A}$ and time is normalized by $\Omega_{\rm p}^{-1}$. Starting from $v_r = 0$, particles are assigned to bins of width dv, where $dv = 0.01$, and are then counted to produce a distribution function f_r (v_r) applied over the entire simulation box at a fixed time. The resulting f_r (v_r) is normalized by the sum of all counts (i.e., $200 \cdot 256^3$) and also by $n_0 V_{\rm A}^3$.

The distribution f_r provides the basis for estimating a gyrotropic distribution perpendicular to $\boldsymbol{B}_0$ along a single coordinate direction. This distribution is denoted by $f_\perp$ and is given by $f_\perp$ $(v_\perp) = f_r/(2\ \pi\ v_{r,1/2}\, dv)$, where $v_{r,1/2}$ is the bin centered speed and $v_\perp = v_{r,1/2}$. Figure 2 shows $f_\perp$ $(v_\perp)$ at $t = 200$ during the quasi-steady phase of the turbulence using a solid line. The dashed line in the plot is the equivalent Maxwellian distribution based on the perpendicular thermal speed $v_{\rm ther,\perp} = 0.33$ at $t = 200$. The obtained gyrotropic distribution function has a maximum about zero speed, but otherwise differs from the equivalent Maxwellian. There are fewer particles about zero speed and at high plotted speeds than for the Maxwellian, and more particles near the thermal speed.

From the lowest speeds, the addition of heat to the protons can be compared to a model of diffusion. Diffusion would act to redistribute greater concentrations of protons at lower speeds to higher speeds through heat addition.

The change in $f_\perp$ with time is modeled by

$$\frac{\partial f_\perp}{\partial t} = \frac{1}{v_\perp}\frac{\partial}{\partial v_\perp}\left(v_\perp D_{\perp\perp}\frac{\partial f_\perp}{\partial v_\perp}\right), \tag{1}$$

where $D_{\perp\perp}$ is the perpendicular velocity space diffusion coefficient, normalized by $V_{\rm A}^2\Omega_{\rm p}$, which depends on $v_\perp$ and time t. The equation can be recognized as a diffusion equation

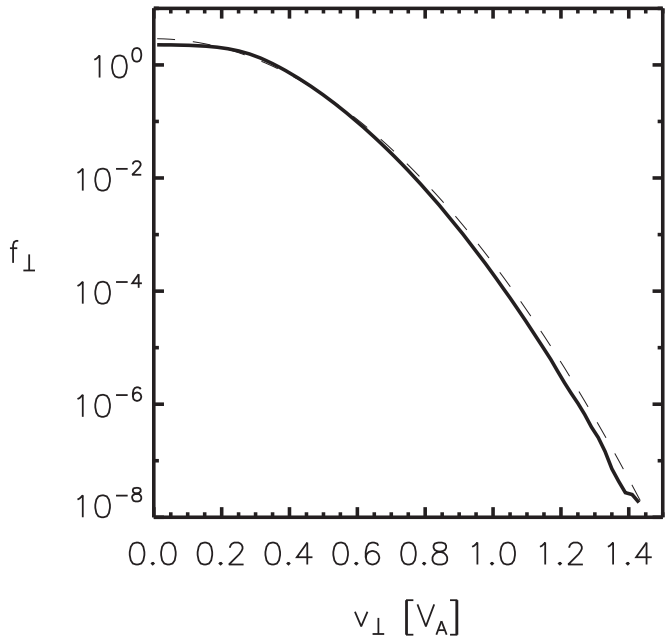

Figure 2. Plot of the gyrotropic averaged distribution $f_\perp$ as a function of $v_\perp$. The solid line shows $f_\perp$ at $t = 200$. The dashed line is a plot of a Maxwellian function $\pi^{-1}v_{\mathrm{ther},\perp}^{-2}e^{-v_\perp^2/v_{\mathrm{ther},\perp}^2}$ for $v_{\mathrm{ther},\perp} = 0.33$.

in cylindrical coordinates with $v_\perp$ in place of the radius. Since the simulation provides $f_\perp$ ($v_\perp$), $D_{\perp\perp}$ is sought.

Below, two numerical methods to fit $D_{\perp\perp}$ are described, and then fits from simulation results and comparison with predictions are made. Section 3.1 fits $D_{\perp\perp}$ using Equation (1) directly, which is a differential equation, and this approach is referred to as method I. Section 3.2 presents method II, which develops an integro-differential equation to fit $D_{\perp\perp}$ that can complement method I and is especially useful if higher-order accuracy is needed. Section 3.3 describes the $D_{\perp\perp}$ found from our simulation, while Section 3.4 compares that $D_{\perp\perp}$ with predictions based on particular mechanisms of turbulence dissipation.

3.1. Method I: Fitting with Differential Equation

To obtain $D_{\perp\perp}$ from the time evolution of $f_\perp$ ($v_\perp$), we use a finite difference representation of Equation (1) based on the second-order velocity space and first-order time accurate implicit approach. (A Crank–Nicholson scheme that provides second-order time accuracy gives similar results to those reported here.) The velocity derivative is evaluated using a uniform grid with cell width Δv, designating $f_\perp$ at midpoints between grid points and $D_{\perp\perp}$ at grid points. In general, the midpoint approach conserves the number density with time when $2\pi v_\perp f_\perp \Delta v$ is summed over all grid points. The grid points are indexed by i and run from $i = 0$ where $v_\perp = 0$ to $i = N_r$ where $f_\perp$ approaches zero. The index for time is given by n. The discretization of Equation (1) at the $i + 1/2$ index and time level n is given by

$$\frac{\Delta_t f_{\perp,i+1/2}}{\Delta t} = \frac{v_{\perp,i}D_{\perp\perp,i}\Delta_v^- f_{\perp,i+1/2}}{v_{\perp,i+1/2}(\Delta v)^2} + \frac{v_{\perp,i+1}D_{\perp\perp,i+1}\Delta_v^+ f_{\perp,i+1/2}}{v_{\perp,i+1/2}(\Delta v)^2}, \quad (2)$$

where

$$\Delta_t f_{\perp,i+1/2} = f_{\perp,i+1/2,n} - f_{\perp,i+1/2,n-1}, \quad (3)$$

$$\Delta_v^- f_{\perp,i+1/2} = f_{\perp,i-1/2,n} - f_{\perp,i+1/2,n}, \quad (4)$$

and

$$\Delta_v^+ f_{\perp,i+1/2} = f_{\perp,i+3/2,n} - f_{\perp,i+1/2,n}. \quad (5)$$

By symmetry $f_{\perp,-1/2,n}$ equals $f_{\perp,1/2,n}$. The values of $D_{\perp\perp}$ are at the nth time. Equation (2) can be solved for $D_{\perp\perp,i+1}$ as

$$D_{\perp\perp,i+1} = -\frac{v_{\perp,i}D_{\perp\perp,i}}{v_{\perp,i+1}}\frac{\Delta_v^- f_{\perp,i+1/2}}{\Delta_v^+ f_{\perp,i+1/2}} + \frac{v_{\perp,i+1/2}}{v_{\perp,i+1}}\frac{(\Delta v)^2}{\Delta t}\frac{\Delta_t f_{\perp,i+1/2}}{\Delta_v^+ f_{\perp,i+1/2}}. \quad (6)$$

To evaluate Equation (6), the time difference Δt must be sufficiently large so that the distributions are distinguishable. Near $v_\perp = 0$, the difference between $f_\perp$ at $v_{\perp,1/2}$ and at $v_{\perp,3/2}$ will generally be small, and as such this region about $v_\perp = 0$ imposes the limits on the velocity space resolution needed to determine $D_{\perp\perp}$. For the present analysis, $\Delta v_\perp = 0.02$ and $\Delta t = 40$ are used in the case of the distribution in Figure 2 at $t = 200$.

The value of $D_{\perp\perp,1}$ can be found without knowing $D_{\perp\perp,0}$, assuming that $v_\perp D_{\perp\perp,0}$ vanishes in the limit of $v_\perp = 0$. From here the value of $D_{\perp\perp,i}$ for successively larger $v_\perp = i\Delta v$ can be calculated from the value at $i - 1$. Finally, the value of $D_{\perp\perp,0}$ can be determined by extrapolating from neighboring $D_{\perp\perp}$ values and by using as a boundary condition $\partial D_{\perp\perp}/\partial v_\perp = 0$ at $v_\perp = 0$.

The evaluation of $D_{\perp\perp,i+1}$ from Equation (6) can be marched out from $i = 0$ through a continuous range of nonzero $f_{\perp,i+1/2}$. The evaluation ends at the first occurrence of $f_{\perp,i+1/2} = 0$. As a practical manner, bins with very few particles from the simulation could generate bins with no particles interspersed with those that have a few at the highest occupied speeds. At this point, finite differences of $f_\perp$ would certainly not be accurate and so there would be no reason to continue the calculation of $D_{\perp\perp,i+1}$.

The diffusive model is applicable where $D_{\perp\perp}$ is positive definite over the range where $f_\perp$ is determined to be significant. The case of interest here for $f_\perp$ would be one where it decreases monotonically with increasing $v_\perp$; any deviations from that would occur only where $f_\perp$ becomes affected by numerical uncertainties. In this case, the first term in Equation (6) is greater than zero if $D_{\perp\perp,i} > 0$. The second term in Equation (6) has a sign that depends on $\Delta_t f_{\perp,i+1/2}$ and is negative if $\Delta_t f_{\perp,i+1/2} > 0$ and positive if $\Delta_t f_{\perp,i+1/2} < 0$. Thereby, a negative diffusion coefficient would result if both $\Delta_t f_{\perp,i+1/2} > 0$ and the magnitude of the second term is greater than the first term.

Finding a negative coefficient could lead to a rejection of the diffusion model for the case at hand. However, the rejection should be made only after testing different Δv and Δt to see if the situation can be remedied. If acceptable values can be found, then those should be used for neighboring times to see if parameters hold consistently. If the results are not consistent, then the evolution of $f_\perp$ is potentially nondiffusive in at least some aspects of that evolution. From here the accuracy of the scheme could be increased for further tests, such as with a Crank–Nicholson approach for time accuracy or with even

higher-order schemes for velocity space derivatives. The recommended approach, however, is to use method II in which the higher-order schemes are more readily implemented. Additional tests would consider improving $f_\perp$ by conducting simulations with greater numbers of particles per cell. If all these attempts fail, then one could conclude that the evolution of $f_\perp$ is actually nondiffusive to some degree.

3.2. Method II: Fitting with the Integro-differential Equation

Multiplying Equation (1) by $v_\perp$ and integrating over $v_\perp$ yields

$$\int_0^{v_\perp} v' \frac{\partial f_\perp}{\partial t} dv' = v_\perp D_{\perp\perp} \frac{\partial f_\perp}{\partial v_\perp}. \tag{7}$$

The value of $D_{\perp\perp}$ at a particular $v_\perp$ can be assessed from Equation (7) without reference to the coefficient at other $v_\perp$ as occurs in method I. This gives a numerically independent way to find $D_{\perp\perp}$ and to compare results with method I.

A first-order time accurate and second-order velocity space accurate difference scheme for $D_{\perp\perp,i}$ is given by

$$D_{\perp\perp,i} = \frac{(\Delta v)^2}{v_{\perp,i}\Delta t} \frac{\sum_{j=0}^{j=i-1} v_{\perp,j+1/2} \Delta_t f_{\perp,j+1/2}}{f_{\perp,i+1/2,n} - f_{\perp,i-1/2,n}}, \tag{8}$$

for $i \geqslant 1$. The value of $D_{\perp\perp,0}$ is found by extrapolation as employed with method I. The obtained coefficients are all at the nth time.

In the cases examined below, Equation (8) gives nearly the same values as Equation (6). The difference schemes for the derivatives present in Equation (7) could be upgraded to higher accuracy in truncation order by simply substituting the relevant schemes. Method I is more difficult to implement in this regard because high-order velocity space differencing would couple values of $D_{\perp\perp}$ at more than two velocity space points per equation and so generally require the simultaneous solution of these equations.

3.3. Perpendicular Velocity Diffusion Coefficient Found in Simulation Results

Method I is used to examine the evolution of $f_\perp$ from the hybrid simulation results described in Section 2. Figure 3 shows $D_{\perp\perp}$ for the distribution displayed in Figure 2 at $t = 200$. Similar $D_{\perp\perp}$ values are obtained at $t = 160$ and $t = 240$ for $v_\perp < 0.8$. The coefficient approaches a relative maximum at small $v_\perp$ and so is consistent with $\partial D_{\perp\perp}/\partial v_\perp = 0$ at $v_\perp = 0$. Beginning near $v_\perp = 0.3$ and extending to 0.8, the value of $D_{\perp\perp}$ steeply declines with a slope of about -3. A distinct minimum is obtained near $v_\perp = 0.9$ after which $D_{\perp\perp}$ increases steeply toward larger speeds with a slope near 7. The minimum is persistent in time but its value at $t = 160$ and $t = 240$ has $D_{\perp\perp}$ about 3 times that at $t = 200$. So the value of $D_{\perp\perp}$ near the minimum is likely inaccurate to some degree, but is reproducible with different Δv and Δt. Beyond $v_\perp = 1.1$, statistical fluctuations in $D_{\perp\perp}$ and large differences in consecutive values of $D_{\perp\perp}$ occur. Here the inaccuracy in the diffusion coefficient has increased for two reasons. First, the overall particle numbers in the simulation at such speeds are too small to provide the statistics needed to model diffusive-like behavior. Second, the faster particles have larger gyroradii (up to $0.06L_\perp$) and so likely interact with fluctuations of larger scales. The perpendicular wavenumbers $k_\perp$ of these

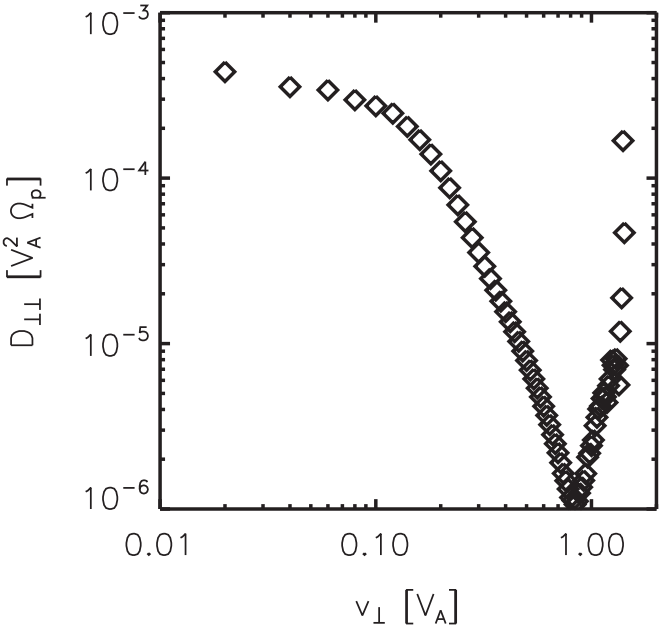

Figure 3. Plot of $D_{\perp\perp}$ as a function of $v_\perp$ at $t = 200$. The value of $D_{\perp\perp}$ has been calculated up to $v_\perp = 1.4$. Method I is used in the calculation. Method II gives similar results, and values for $v_\perp \leqslant 0.9$ differ by less than 0.04% relative to those plotted.

fluctuations are associated with gradients that are of order of the inverse of the gyroradii, and so these fluctuations have $k_\perp \lesssim 1$. The smallest $k_\perp$ represented on the grid is 0.25, so the statistical behavior is likely informed by the finite box size in the simulation.

The appearance of a relative minimum in $D_{\perp\perp}$ is suggestive of the superposition of two distinct sources of diffusion where different processes acting at lower and higher $v_\perp$ intersect. From lower speeds in Figure 3, diffusion arises mostly from turbulence generated fluctuations in the dissipation range and the higher-end inertial range ($k_\perp > 1$). At higher speeds, larger scale fluctuations contribute the most to the diffusion. Since these larger scale fluctuations are few in number and have the largest amplitudes in the simulation box, proton–fluctuation interactions at these scales may be more coherent than those experienced among smaller scale turbulence generated fluctuations. The shortness of the inertial range ($0.5 < k_\perp < 2$) in the simulation makes the distinction between diffusion associated with the coherent-like energy containing scales and the turbulence generated inertial range unclear. However, a more realistic inertial range of considerable extent should be energy conserving and so proton–fluctuation interactions in the inertial range would be associated with little proton heating. Where turbulence generated fluctuations more clearly determine $D_{\perp\perp}$, diffusion for $v_\perp > v_{\mathrm{ther},\perp}$ tends to decrease significantly with increasing $v_\perp$. Extrapolating to an extensive inertial range, the expectation, at present, would have $D_{\perp\perp}$ to continue to decrease at even larger $v_\perp$.

Another representation for the proton behavior considers the energy diffusion coefficient $D_{e,\perp\perp}$ which is defined as $D_{e,\perp\perp} = v_\perp^2 D_{\perp\perp}$. Figure 4 plots $D_{e,\perp\perp}$ as a function of $v_\perp$ for $t = 200$ from the values shown in Figure 3. The value of $D_{e,\perp\perp}$ increases from small speeds to a relative maximum near but below the thermal speed and then decreases to a relative minimum near $v_\perp = 0.9$. At the relative maximum, energy diffusion is most rapid, and protons are most impacted by the

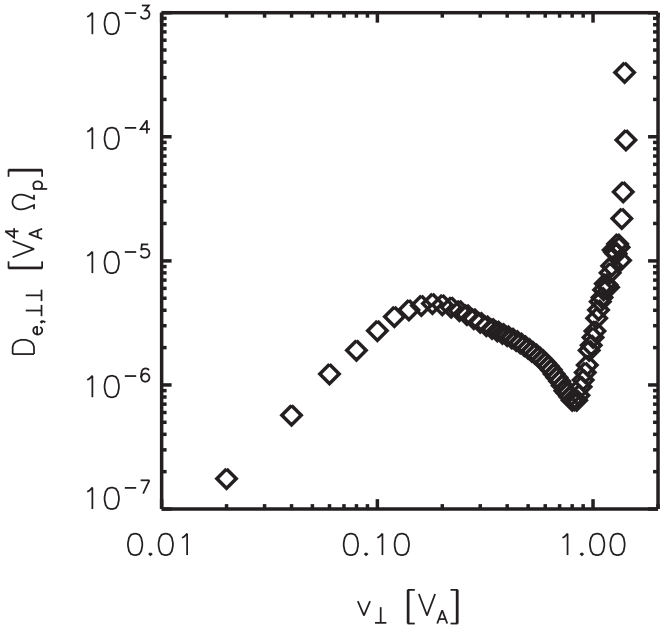

Figure 4. Plot of energy diffusion coefficient $D_{e,\perp\perp}$ as a function of $v_\perp$ at $t = 200$. The plotted $D_{e,\perp\perp}$ is calculated from $v_\perp^2 D_{\perp\perp}$ using the $D_{\perp\perp}$ values in Figure 3.

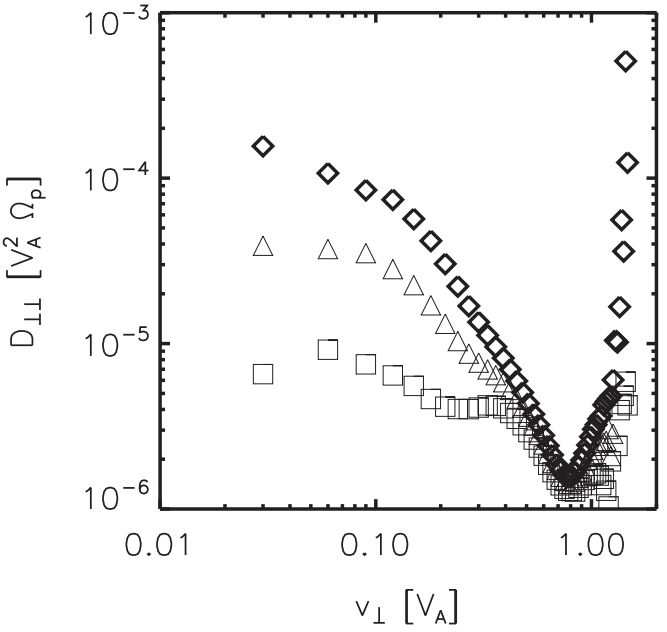

Figure 5. Plot of $D_{\perp\perp}$ as a function of $v_\perp$ for $t = 400$ (diamonds), $t = 480$ (triangles), and $t = 560$ (squares). At $t = 560$ there are two off-scale values of $D_{\perp\perp}$: $D_{\perp\perp}$ ($v_\perp = 1.26$) $= 2 \times 10^{-7}$ and $D_{\perp\perp}$ ($v_\perp = 1.29$) $= 8 \times 10^{-7}$. The range of calculated $D_{\perp\perp}$ is shorter for later times. As the energy cascade diminishes with time, the slowest particles are affected the most whereas protons above the thermal speed ($\approx$0.35) at these times continue to diffuse at nearly the same rate. Method I is used in the calculation.

turbulence. Because the relative maximum is near the thermal speed, the turbulence preferentially heats protons near the thermal gyroradius associated here with fluctuations having $k_\perp \sim 3$. This was the conclusion reached in Vasquez (2015) based on simulations with an additional and competitive source of turbulent dissipation based on an anomalous resistivity.

From $t = 400$ and afterwards, diffusion diminishes and eventually fails to model the evolution of the distribution past $t = 600$. Figure 5 shows the evolution of $D_{\perp\perp}$ during this period. At corresponding times, Figure 1 shows that the thermal energy gain decreases significantly. The decrease is due to the smaller amplitude of the decaying turbulence, which leads to a significant reduction in the energy cascade rate proportional to the amplitude cubed. With slower changes, Equation (6) is evaluated using $\Delta v_\perp = 0.03$ and $\Delta t = 80$ to obtain the plotted results in Figure 5. Between $t = 400$ and 560, $D_{\perp\perp}$ decreases with time for $v_\perp$ below the thermal speed, and the maximum of $D_{\perp\perp}$ about $v_\perp = 0$ eventually disappears. Above the thermal speed, $D_{\perp\perp}$ changes only slowly and maintains its overall form about the minimum near $v_\perp = 0.9$. This behavior is expected since the slower cascade causes the energy at smaller scales to decay first. Thus, the slower diffusion will appear first in the protons with the smallest gyroradii. Sufficient energy does remain above the thermal gyroradius scale where the inertial range is present so as to support continued diffusion. At longer times, application of Equation (6) gives negative $D_{\perp\perp}$ values at low speeds, so that proton evolution becomes potentially nondiffusive.

3.4. Comparison with Theoretical Predictions

To compare these simulation results with currently available theoretical predictions of perpendicular diffusion, we take the coefficient values shown in Figure 3 and consider the behavior between $v_\perp = 0.1$ and 0.7, which contains $v_{\mathrm{ther},\perp} = 0.3$. Below this range, $D_{\perp\perp}$ varies only slowly, and values above this range do not seem to represent processes due to turbulent dissipation.

The values of $D_{\perp\perp}$ between $v_\perp = 0.1$ and 0.7 can be suitably fitted with a form that asymptotes to a power law, with an exponential function of some form, or with a combination of these fitted forms. In this range $D_{\perp\perp}$ varies over two orders of magnitude, but that is not sufficient to determine definitively its actual form.

Isenberg & Vasquez (2019) derived quasilinear proton diffusion coefficients due to resonant interactions with a turbulence-like spectrum of kinetic Alfvén waves. In their idealized model, the kinetic Alfvén waves were described by a two-fluid dispersion relation and the resonances were taken to be infinitesimally narrow. This last assumption is not appropriate to represent turbulence, since it invokes interactions with periodic waves of infinite duration. The authors acknowledged that a more realistic model would use substantially broadened resonances, but at present this work has not been extended.

The idealized kinetic Alfvén waves yield a very strong Landau resonance, but Isenberg & Vasquez (2019) showed that the low β proton response to the Landau interaction would be small. Apart from an initial parallel energization, the proton evolution in that work was dominated by the perpendicular heating caused by the cyclotron resonance. The form of $D_{\perp\perp}$ in that paper (see their Figure 5) has a relative maximum at $v_\perp = 0$ and decreases gradually until $v_\perp \sim 0.1$, above which it approximates a power law with index -1.

A least-squares power-law fit to $D_{\perp\perp}$ in Figure 3 was applied to the subrange $v_\perp = 0.3$ to 0.7 where the power-law fit appears to be more appropriate. The fit yields a slope of -3.2 ± 0.9, which is much steeper than the behavior in Isenberg & Vasquez (2019). It is not clear whether this difference is due to a fundamental discrepancy in the physical mechanism or to a resolvable detail of the theoretical model. For instance, the shape of the diffusion coefficient will depend

on the choice of the turbulence spectrum. It would also be interesting to see if resonance broadening in the quasilinear calculations could yield diffusion coefficients with steeper dependencies on $v_\perp$.

Klein & Chandran (2016) derived a prediction for the energy diffusion coefficient $D_{e,\perp\perp}$ based on turbulent dissipation due to stochastic heating or magnetic moment breaking of protons. The particular form was based on an inertial range that obeyed an Iroshnikov–Kraichnan (IK) spectral power law with index $-3/2$ (Iroshnikov 1963; Kraichnan 1965). Using the IK form, the equivalent velocity diffusion coefficient for stochastic heating gives $D_{\perp\perp} \propto v_\perp^{-1/4} \exp(-d_{\rm IK} v_\perp^{3/4})$, where $d_{\rm IK}$ is a constant. The value of $d_{\rm IK}$ is related to the c_2 constant present in the Chandran et al. (2010) cascade rate predictions and is given by $d_{\rm IK} = c_2/A_v k_0^{1/4}$, where A_v is the rms velocity amplitude normalized by $V_{\rm A}$, and k_0 is the outer scale perpendicular wavenumber normalized by $(c/\omega_{\rm pp})^{-1}$. For the simulations here, k_0 equals 0.25, which is the wavenumber of the largest perpendicular wavelength represented on the simulation grid. At $t = 200$, we find $A_v = 0.09$. Klein & Chandran (2016) consider the relevant value of c_2 for their work to be 0.2 where this value for c_2 is the best estimate gained from test particle calculations involving phase-random Alfvénic waves (Xia et al. 2013). This then yields $d_{\rm IK} = 3.14$ for the simulation results.

From the values of $D_{\perp\perp}$ in Figure 3 in the range of $v_\perp = 0.1$ and 0.7, a fit has been made to the functional form $v_\perp^{-1/4} \exp(-d_{\rm IK} v_\perp^{3/4})$. This fit finds $d_{\rm IK} = 7.7 \pm 1.0$. The simulation determined $D_{\perp\perp}$ does decrease far faster with $v_\perp$ than does the prediction. The value of $c_2 (= A_v k_0^{1/4} d_{\rm IK})$ for simulation results is 0.49. In the limit $v_\perp = 0$, the predicted form has the coefficient approaching infinity but would still satisfy the condition $v_\perp D_{\perp\perp} \to 0$ as $v_\perp \to 0$ used in method I. Klein & Chandran (2016) noted that a steepening of the IK spectral form in a small-scale dissipation range would prevent this infinite limit as $v_\perp \to 0$ (see also Isenberg et al. 2019).

Taking a Kolmogorov spectrum with power-law index 5/3 modifies the above prediction so that the coefficient near $v_\perp = 0$ behaves in a regular manner. This approach better suits the simulations because the inertial range power spectrum in the simulation has a slope that approximately matches the Kolmogorov prediction and the determined proton heating rate also follows a generalized Kolmogorov prediction (Vasquez 2015). For the Kolmogorov case, stochastic heating gives $D_{\perp\perp} \propto \exp(-d_{K41} v_\perp^{2/3})$, where $d_{K41} = c_2/A_v k_0^{1/3}$. Using $c_2 = 0.2$ and simulation values for A_v and k_0, the expected d_{K41} is 2.65. When $D_{\perp\perp}$ in Figure 3 is fitted with this form, d_{K41} is found to be 8.7 ± 1.1, implying $c_2 = 0.49$. Thus, the difference with the Kolmogorov prediction remains about the same as for the IK prediction.

Considering all the test particle calculations made in Xia et al. (2013), c_2 ranges anywhere from $c_2 = 0.15$ to 0.44. Thus, at the upper end of the range of values, the difference with the simulation would appear to be small. However, there may not be a true match between the constant in the exponential term and c_2 with regards to the present self-consistent kinetic simulations. Vasquez (2015) directly sought c_2 by evaluating the proton heating rate as a function of rms amplitude and found no discernible exponential cutoff at appropriately small amplitudes, implying that c_2 is negligible. In self-consistent simulations, nonlinearity at large scales determines the rate of energy cascade toward small scales, and the electromagnetic fields at the small scales are reactive to the incoming energy cascade. The electromagnetic fields at the small scales then adjust to the energy cascade and can develop a statistical steady state wherein the rate of exchange between electromagnetic energy and proton thermal energy matches the cascade rate. Test particle calculations, such as those in Xia et al. (2013), use specified electromagnetic fields and so are not reactive.

4. Comparison with Arzamasskiy et al.'s Approach

Arzamasskiy et al. (2019) estimated the proton perpendicular energy diffusion coefficient $D_{e,\perp\perp}$ for the turbulent heating in their simulations. To follow their method, let $W = v_\perp^2/2$, where W is a kinetic energy per unit mass, and transform Equation (1) to

$$\frac{\partial f_\perp}{\partial t} = \frac{\partial}{\partial W}\left(D_{e,\perp\perp} \frac{\partial f_\perp}{\partial W} \right). \tag{9}$$

A quantity $Q_\perp$ is then defined that is proportional to the perpendicular energization rate per unit mass with an indefinite integral by

$$Q_\perp \equiv \int W \frac{\partial f_\perp}{\partial t} dW, \tag{10}$$

so that $\partial Q_\perp/\partial W$ is given by

$$\frac{\partial Q_\perp}{\partial W} = W \frac{\partial f_\perp}{\partial t}. \tag{11}$$

Multiplying both sides of Equation (9) by W finds $\partial Q_\perp/\partial W$ as

$$\frac{\partial Q_\perp}{\partial W} = W \frac{\partial}{\partial W}\left(D_{e,\perp\perp} \frac{\partial f_\perp}{\partial W} \right). \tag{12}$$

In Arzamasskiy et al. (2019) an expression is pursued by integrating over W and evaluating the right-hand side through integration by parts. Central to integration by parts is the expansion of the right-hand side in accord with the chain rule. Hence, Equation (12) can be rewritten as

$$\frac{\partial Q_\perp}{\partial W} = \frac{\partial}{\partial W}\left(W D_{e,\perp\perp} \frac{\partial f_\perp}{\partial W} \right) - D_{e,\perp\perp} \frac{\partial f_\perp}{\partial W}. \tag{13}$$

Arzamasskiy et al. (2019) effectively evaluate $D_{e,\perp\perp}$ from (13) by using assessed values of $\partial Q_\perp/\partial W$ and $\partial f_\perp/\partial W$ but neglecting the first term on the right-hand side. Moreover only the magnitude of $D_{e,\perp\perp}$ was obtained because the sign of the $\partial Q_\perp/\partial W$ as a function of W was not considered. Because the adopted relation for $D_{e,\perp\perp}$ is a differential equation, the results in Arzamasskiy et al. (2019) will be compared to results obtained with method I.

Generally, diffusion from lower to higher speeds occurs such that particles are lost at low speeds and gained at higher speeds. In the turbulence simulations this occurs about $v_{{\rm ther},\perp}$ where the energy change from particles lost or gained passes through zero, implying that $\partial Q_\perp/\partial W$ changes sign there. With the method in Arzamasskiy et al. (2019), the magnitude of $D_{e,\perp\perp}$ has a relative minimum near the thermal speed. If the sign were retained, $D_{e,\perp\perp}$ would have been negative for $v_\perp < v_{{\rm ther},\perp}$ and positive above. When all terms are retained, as used for the calculation of $D_{e,\perp\perp}$ in Figure 4 by method I, $D_{e,\perp\perp}$ is positive throughout and is near a relative maximum at $v_{{\rm ther},\perp}$.

It will be interesting to see the behavior of the diffusion coefficient from the Arzamasskiy et al. simulations, as obtained through one of the methods presented in Section 3.

5. Production of Suprathermal Protons

Interplanetary turbulence features an extensive inertial range of over three decades. If the associated turbulence velocity diffusion coefficient falls off with increasing $v_\perp$ as steeply as a power law with index -3, then even the energy diffusion coefficient decreases with index -1. Even less diffusion could be expected at larger $v_\perp$ if the coefficient is exponentially decreasing.

An implication of the above fall off is that protons substantially beyond $v_{\mathrm{ther},\perp}$ would not be readily accelerated. In the solar wind, suprathermal ions form a tail with respect to the thermal population and can be injected into acceleration processes that produce energetic particles in the solar wind (e.g., Gosling et al. 1981; Dayeh et al. 2009). The time τ for velocity diffusion for suprathermals can be estimated from our simulation results by taking a few steps to rescale them. First, take the dimensional value of $D_{\perp\perp}$ at $v_{\mathrm{ther},\perp} = 0.3$ in Figure 3, which is $5 \times 10^{-5} V_{\mathrm{A}}^2 \Omega_{\mathrm{p}}$. Second, note that the simulation uses about twice the amplitude for fluctuations at comparable scales as found in fast winds, where amplitudes are generally greatest. The diffusion rate should vary with the cube of amplitude in accord with the heating and cascade rate found in simulations, and so the coefficient magnitude in the solar wind is 8 or more times smaller. Lastly, the diffusion coefficient for $v_\perp > v_{\mathrm{ther},\perp}$ can be treated as a power law with index -3 since an exponential would yield even less diffusion. With these steps, the solar wind diffusion coefficient $D_{\perp\perp}^{\mathrm{SW}}$ at large speeds can be expressed by

$$D_{\perp\perp}^{\mathrm{SW}} \lesssim 1.7 \times 10^{-7}\, v_{\star,\perp}^{-3}\, V_{\mathrm{A}}^5\, \Omega_{\mathrm{p}}, \tag{14}$$

where $v_{\star,\perp}$ is the dimensional speed. This estimate specifically applies to solar wind plasmas with $\beta_{\mathrm{p},\perp}$ near 0.1. The diffusion time τ can be estimated from $\tau \sim v_{\star,\perp}^2 / D_{\perp\perp}^{\mathrm{SW}}$, which would correspond to the time needed to significantly alter a velocity distribution from a Maxwellian distribution to one with a suprathermal tail. Using Equation (14), the resultant time can be expressed by

$$\tau \gtrsim 5.9 \times 10^6\, \frac{v_{\star,\perp}^5}{V_{\mathrm{A}}^5}\, \Omega_p^{-1}. \tag{15}$$

At 1 au, suprathermals have speeds more than about 4 times larger than V_{A}, and Ω_{p} is about 0.5 s^{-1}. With these values, τ in Equation (15) is greater than 380 yr. It would appear that quasi-perpendicular Alfvénic fluctuations that evolve in broadband (nonshock) turbulence could not contribute significantly to the suprathermal proton population.

Future simulations can make progress in understanding suprathermals by establishing whether or not the form of $D_{\perp\perp}$ due to turbulence generated fluctuations continues to decrease with increasing $v_\perp$ when the inertial range is extensive. The required simulations will need large grid sizes, especially for $L_\perp$, so as to separate better the dissipation and energy containing scales. Simulations with large β_{p} and thermal speeds will also need the larger grid sizes so as not to overlap these scales. With a warm electron plasma, more significant proton parallel heating occurs, and diffusion associated with this energization should also be considered (Parashar et al. 2014). Heavier and minor ions may be accelerated differently than protons, and so the diffusion of these ions should also be investigated.

6. Summary

Hybrid simulation results for proton velocity distributions averaged over the entire grid have been examined for a case of quasi-perpendicular Alfvénic turbulence. The heating of protons in the simulation occurs mainly in the direction perpendicular to the background magnetic field. The averaged perpendicular distribution function was transformed to a gyrotropically average distribution. The evolution of the gyrotropic distribution with time was then modeled with Equation (1) for velocity space diffusion. A method that derives the perpendicular velocity diffusion coefficient $D_{\perp\perp}$ from the differential equation, given by Equation (1), was developed along with an additional method using an integro-differential equation. Results from each method agree well with one another. These methods correct the procedure of Arzamasskiy et al. (2019). During the quasi-steady phase of the turbulence, the simulation case presented here gives a diffusion coefficient that is positive, and so proton kinetics are adequately described as diffusive during that phase.

The value of $D_{\perp\perp}$ as a function of $v_\perp$ was determined from a case considered in Vasquez (2015) with $\beta_{\mathrm{p}} = 0.1$. The form of $D_{\perp\perp}$ has a relative maximum of about $v_\perp = 0$ but decreases around the thermal speed $v_\perp = 0.3$ (in units of V_{A}) approximately according to a power law with index -3. This decreasing portion of $D_{\perp\perp}$ may also be fitted with steep exponential functions. A relative minimum is reached near $v_\perp = 0.9$ beyond which the value rises rapidly but soon becomes inaccurate due to the lack of higher speed particles in the simulation. The corresponding energy diffusion coefficient $D_{e\perp\perp}(=v_\perp^2 D_{\perp\perp})$, from small $v_\perp$ increases to a relative maximum near $v_\perp = 0.2$ and then decreases as a power law with index -1 until reaching the relative minimum near $v_\perp = 0.9$.

The form of $D_{\perp\perp}$ is suggestive of the occurrence of two sources of diffusion whose associated functional dependencies on $v_\perp$ intersect near the relative minimum. From $v_\perp < 0.9$, turbulence generated fluctuations contribute more to diffusion while from $v_\perp > 0.9$ the energy containing fluctuations are mainly promoting the diffusion. With this interpretation, the portion of $D_{\perp\perp}$ due to turbulence would be expected to continue to decrease beyond $v_\perp = 0.9$ as it does from smaller $v_\perp$. When the form of $D_{\perp\perp}$ between $v_\perp = 0.1$ and 0.7 is compared to theoretical models (Klein & Chandran 2016; Isenberg & Vasquez 2019), it found to be significantly steeper than predicted by either model. The steepness of $D_{\perp\perp}$, when it is assumed to continue to large $v_\perp$, could also limit the contribution of quasi-perpendicular turbulence to the formation of suprathermal protons in the solar wind.

The authors are grateful for valuable communications with L. Arzamasskiy and M. Kunz. B.V. and S.M. were supported by the NASA Solar and Heliospheric Physics grant 80NSSC19K0832 to the University of New Hampshire (UNH). B.V. and P.I. were supported by both NASA Heliophysics Grand Challenges Research grant 80NSSC17K0009 and Solar and Heliospheric Physics grant 80NSSC18K1215 to UNH. The simulation results were obtained from the Cray XE6m-200 supercomputer Trillian at UNH. Trillian was purchased and administered with the support of NSF MRI grant PHYS-1229408 to UNH.

ORCID iDs

Bernard J. Vasquez https://orcid.org/0000-0001-8593-7289
Philip A. Isenberg https://orcid.org/0000-0003-0505-8546

References

Arzamasskiy, L., Kunz, M. W., Chandran, B. G. D., & Quataert, E. 2019, ApJ, 879, 53
Chandran, B. D. G., Li, B., Rogers, B. N., Quataert, E., & Germaschewski, K. 2010, ApJ, 720, 503
Cho, J., & Vishniac, E. T. 2000, ApJ, 539, 273
Coburn, J. T., Smith, C. W., & Vasquez, B. J. 2012, ApJ, 754, 93
Cranmer, S. R., & van Ballegooijen, A. A. 2005, ApJS, 156, 265
Dayeh, M. A., Desai, M. I., Dwyer, J. R., et al. 2009, ApJ, 693, 1588
Dmitruk, P., Matthaeus, W. H., Milano, L. J., et al. 2003, ApJ, 575, 571
Gosling, J. T., Asbridge, J. R., Bame, S. J., Feldman, W. C., & Zwickl, R. D. 1981, JGR, 86, 547
Hamilton, K., Smith, C. W., Vasquez, B. J., & Leamon, R. J. 2008, JGR, 113, A01106
Hellinger, P., Trávníček, P. M., Štverák, Š., Matteini, L., & Velli, M. 2013, JGR, 118, 1351
Hollweg, J. V. 1986, JGR, 91, 4111
Hollweg, J. V., & Johnson, W. 1988, JGR, 93, 9547
Iroshnikov, P. S. 1963, AZh, 40, 742 [English transl. 1964 SvA, 7, 566]
Isenberg, P. A., & Vasquez, B. J. 2009, ApJ, 696, 591
Isenberg, P. A., & Vasquez, B. J. 2011, ApJ, 731, 88
Isenberg, P. A., & Vasquez, B. J. 2015, ApJ, 808, 119
Isenberg, P. A., & Vasquez, B. J. 2019, ApJ, 887, 63
Isenberg, P. A., Vasquez, B. J., & Hollweg, J. V. 2019, ApJ, 870, 119
Kennel, C. F., & Engelmann, F. 1966, PhFl, 9, 2377
Klein, K. G., & Chandran, B. D. G. 2016, ApJ, 820, 47
Kohl, J. L., Noci, G., Antonucci, E., et al. 1998, ApJL, 501, L127
Kraichnan, R. H. 1965, PhFl, 8, 1385
Lamarche, L. J., Vasquez, B. J., & Smith, C. W. 2014, JGRA, 119, 3267
Leamon, R. J., Smith, C. W., Ness, N. F., Matthaeus, W. H., & Wong, H. K. 1998, JGR, 103, 4775
Marsch, E., Mühlhäuser, K.-H., Rosenbauer, H., & Schwenn, R. 1983, JGR, 88, 2982
Marsch, E., Mühlhäuser, K.-H., Schwenn, R., et al. 1982, JGR, 87, 52
Matthaeus, W. H., Oughton, S., Ghosh, S., & Hossain, M. 1998, PhRvL, 81, 2056
Oughton, S., Priest, E. R., & Matthaeus, W. H. 1994, JFM, 280, 95
Parashar, T. N., Shay, M. A., Cassak, P. A., & Matthaeus, W. H. 2009, PhPl, 16, 032310
Parashar, T. N., Vasquez, B. J., & Markovskii, S. A. 2014, PhPl, 21, 022301
Shebalin, J. V., Matthaeus, W. H., & Montgomery, D. 1983, JPlPh, 29, 525
Smith, C. W., Vasquez, B. J., & Hollweg, J. V. 2012, ApJ, 745, 8
Stawarz, J. E., Smith, C. W., Vasquez, B. J., Forman, M. A., & MacBride, B. T. 2009, ApJ, 697, 1119
Vasquez, B. J. 2015, ApJ, 806, 33
Vasquez, B. J., & Markovskii, S. A. 2012, ApJ, 747, 19
Vasquez, B. J., Markovskii, S. A., & Chandran, B. D. G. 2014, ApJ, 788, 178
Vasquez, B. J., Smith, C. W., Hamilton, K., MacBride, B. T., & Leamon, R. J. 2007, JGRA, 112, A07101
Verma, M. K., Roberts, D. A., & Goldstein, M. L. 1995, JGR, 100, 19839
Xia, Q., Perez, J. C., Chandran, B. D. G., & Quataert, E. 2013, ApJ, 776, 90
Yang, Y., Matthaeus, W. H., Parashar, T. N., et al. 2017, PhPl, 24, 072306